

ASSESSMENT OF ALKALI-SILICA REACTION IN SOME CONCRETES FROM BRAZILIAN HYDROELECTRIC POWER PLANTS

Nicole P. Hasparyk^{1*}, Patrícia N. Silva², Danilo G. Batista³, Heloísa H. A. B. Silva¹, Helena Carasek³, Alberto J. C. T. Cavalcanti²

¹ELETROBRAS Furnas, Gerência de Pesquisa, Serviços e Inovação Tecnológica, Goiânia, GO, BRAZIL

²Companhia Hidro Elétrica do São Francisco - CHESF, Recife, PE, BRAZIL

³Universidade Federal de Goiás - UFG, Goiânia, GO, BRAZIL

Abstract

Considering that the alkali-aggregate reaction (AAR) had already been diagnosed in several Brazilian hydroelectric power plants, it is important to continue the studies in order to monitor concrete behavior over the years and also to assist in remedial measures when necessary and in future mathematical models. Previous studies conducted in concretes of some structures of those plants have contributed significantly to the analysis of the behavior of the AAR over the years, with their various field investigations and extraction campaigns. The analysis of the characteristics and properties of concrete in different areas through continuous monitoring is very important as source of data about quality and durability of concrete. Considering the above, this paper aims to present a current overview of specific practical investigations in some concretes of five Brazilian hydroelectric plants from Chesf and Furnas. These studies were performed within the Furnas ANEEL R&D Program, and involved from field inspections to tests and analyses at laboratory.

Keywords: HPP, concrete, alkali-aggregate reaction, quality, durability.

1 INTRODUCTION

Furnas and Chesf are electric power companies owned by ELETROBRAS, a mixed-economy company and open-capital stock corporation. The Brazilian Federal Government is the main stockholder. Both construct and/or operate and maintain several hydroelectric power plants.

Furnas and Marechal Mascarenhas de Moraes Hydroelectric Power Plants (HPP) are two of several plants from Furnas Company. Furnas HPP is situated in the state of Minas Gerais; its construction began in 1958 and its reservoir was filled in 1963. Six generating units began to operate between 1963 and 1965. After 1973, Furnas HPP received two more generating units increasing its capacity to 1,216,000 kW. Marechal Mascarenhas de Moraes HPP is located between the state of São Paulo and state of Minas Gerais. In 1950 and 1957, its construction and generation began, respectively. This HPP presents nowadays ten generating units with a total capacity of 476 MW.

The first symptoms of AAR in Furnas HPP were detected in 1976, after about 13 years from the end of its construction. Some of the main observations include vertical displacements measured by topographic levelling at the crest of the concrete blocks, map cracking on spillway pillars, penstocks anchor blocks and Power house. Since then, the concrete structures were monitored more carefully. At Mascarenhas, the first internal technical reports relating this problem date from 1994, later published in 1997.

Paulo Afonso Hydroelectric Complex, from Chesf, comprises five Plants – Paulo Afonso I, Paulo Afonso II, Paulo Afonso III, Paulo Afonso IV (PA I, II, III and IV) located in the state of Bahia, and Moxotó, between the states of Bahia and Alagoas. The construction of Paulo Afonso I began in March 1949, and started commercial operation of power supply in 1954. The construction of Paulo Afonso II began in 1955. Three units of 75 MW are operating since 1961 and another three units of 85 MW each, are operating since 1967. Paulo Afonso III construction started in 1967 and is in operation since 1971. Paulo Afonso IV was built between 1975 and 1979. Its reservoir was filled in August 1979 and its six Francis-type turbines with a rated horsepower of 410 MW per unit went into

* Correspondence to: nicolepha@gmail.com

operation between December 1979 and May 1983. The Apolônio Sales (Moxotó) Power Plant was built between 1972 and 1977. Since the early stage of the commercial exploitation, the units presented an abnormal performance with progressive shifting and tilting of the turbine shaft.

The first AAR symptoms in the Chesf Hydroelectric Complex were observed at the end of the 70s in Paulo Afonso II, when the plant had cumulated 17 years of operation. Since then, the evidence of AAR in the structures of the Plants became clearer, including: concrete cracking, differential displacements at contraction joints and crushing of small concrete columns that supported cable trays. Evidences of AAR in Moxotó Plant date from 1979, when a whole series of cracks in its walls and slabs had started to draw the attention of Chesf's technicians, just two years after Plant first operation. During the operational period, several anomalies were identified in the hydro generating units of Moxotó Plant, and in 1984 the suspicion of AAR existence was confirmed, leading Chesf to carry out extensive investigations. Some concrete cores were extracted from PA I, PA II, PA III, PA IV and Moxotó plants for petrographic analyses in order to confirm the presence of AAR. The report stated that AAR was present in the concrete and diagnosed strained quartz as the main reactive mineral. The investigation program concluded that the cause of the problems was the alkali-silica reaction (ASR) due to the combination of granite aggregates and high alkali cement used in the construction.

This paper presents the results of more recent investigations carried out on concrete cores drilled from five HPPs: Furnas, Mascarenhas, PA II, PA IV and Moxotó Power Plants.

2 MATERIALS AND METHODS

Experiments performed on concretes and aggregates from Brazilian HPPs were part of Furnas ANEEL R&D Program, and involved from field inspections to laboratory tests. This paper presents the results from lab tests.

2.1 Materials

After visiting the HPPs, some field investigations and several visual inspections on concrete surfaces, sites for concrete drilling were selected from drainage galleries. Some sampling of aggregates surrounding the HPPs was also done. Concrete cores were extracted using a drill (ZWF) with a hollow barrel tipped with industrial diamonds, with 152 mm internal diameter and 500 mm of free internal length. All drilled cores had a maximum length of 45 cm so that after the edges were cut off, they would remain with a size of approximately 15 cm in diameter x 30 cm in length, so they could undergo mechanical tests. In total, 37 cores were extracted. The concrete samples studied in this research are detailed in Table 1.

Exudation products were collected at the surface of concrete elements for further analysis in the laboratory, except for Moxotó.

2.2 Methods for assessment and analysis

After sampling and drilling concretes, several tests and analyses were performed in the laboratory, as described below.

Characterization of concrete core aggregates and HPP surrounding rocks

Some concrete core samples were selected from each HPP to carry out petrographic analysis aiming to determine not only the nature and lithotype of the aggregates, but also mineralogical features related to alkali-aggregate reactivity (NBR 15577/3)[1], among other significant aspects. For this purpose, polished thin sections were prepared and studied under transmitted light in a polarizing microscope (Opton, Model: Eclipse E200Pol).

A systematic sampling at the sites of the studied HPPs was also conducted to carry on petrographic analysis in order to get a better comprehension of the rock itself and mainly, the transformations or possible reactions that might have happened with the aggregates inside de concrete during all these years.

Mechanical tests of concretes

Mechanical tests were performed on the drilled concrete cores. Compressive strength and modulus of elasticity tests were performed following the main prescriptions from ASTM Standards C39 and ASTM C469 [2,3], respectively. The elastic modulus test was determined using the same sample than the compressive strength test, at 40% of the compressive strength determined in the test. The loading speed during the test was 0.25 MPa/s, in accordance with ASTM C-39 recommendations. An electromechanical testing machine was used along with strain gages with 100-mm gage lengths.

Chemical tests of concrete

Chemical tests were carried out in order to detect and quantify specially the alkali contents in concretes. Those alkalis were determined by atomic absorption spectrometry. In order to obtain sample for analysis, coarse aggregates were visually and physically separated from mortars followed by crushing and grinding of both portions individually. Aggregates have suffered no cleaning in this process; it was done a simple and rough separation. Samples passing the 150 μm mesh sieve from each portion (mortar / coarse aggregates) were then attacked by hydrochloric acid at boiling point and readings of **total alkalis** (Na^+ and K^+ ionic concentration) were collected from spectrometry. Considering this procedure, some alkalis can be probably released from aggregates. **Soluble alkalis** followed the same procedure, but attack was performed just in distilled water at boiling point for 5 minutes, standing at room temperature for 24 hours.

The pH determination from concrete cores was also investigated. For this purpose, the procedure presented in [4] was adapted in this study. First of all, mortars from concrete cores were physically separated followed by its powdering by using agate grinder. After that, the material was sieved under 150 μm . In the sequence, deionized water at 22°C was added in about 5 g of powdered material and mixture was stirred for dissolution of the soluble hydroxides and alkalis present of concretes. The filtration was undergone and pH measurements performed using a pH Meter.

Expansion tests on aggregates

Potential reactivity of the aggregates was studied through accelerated method in mortar bars. Expansion tests followed the test method (AMBT), according to Brazilian standard NBR 15577-4 [5], which is similar to ASTM C1260[6], in the presence of a standard free-of-admixtures reference cement with the following oxide composition: SiO_2 19.52wt%, CaO 62.33wt%, Al_2O_3 4.80wt%, Fe_2O_3 2.26wt%, MgO 1.90wt%, SO_3 3.64wt%, with 0.87wt% and 0.32wt% potassium and sodium total alkali, respectively ($\text{Na}_2\text{O}_{\text{eq}}$ 0.87wt%). Cement fineness was equal to 4,920 cm^2/g and autoclave expansion of 0.02%.

The tests were conducted over 30 days, in two steps as follows:

Expansion of rocks – this test was performed with rocks sampled from nearby the power plants, but after construction: the rock material was collected in regions near each of the power plants studied, and processed to obtain manufactured sand from crushed rock.

Expansion of concrete aggregates - this test was performed with aggregates extracted from the interior of the concrete cores drilled from HPPs. After the concrete mechanical tests; the samples were fractured in order to separate the aggregates for later processing to obtain manufactured sand from coarse aggregates. The particle size of the coarse aggregates in the concrete cores varied from one structure to the other. Furnas, Mascarenhas and Paulo Afonso II have presented 152 mm as maximum size of drilled concrete aggregates, while Paulo Afonso A IV and Moxotó, 76 mm and 38 mm, respectively.

Petrographic investigations on concretes and gels

The concrete core samples were carefully visually examined after the mechanical tests and then prepared for microstructural analyses under the scanning electron microscope (SEM) coupled with energy dispersive X-ray spectrometry (EDS). Samples were prepared with fracture surfaces and the coating was performed in a gold sputter. Mortar samples from concretes were also investigated by X-ray diffraction. All analyses were conducted in order to assess the chemical alterations and the neoformed products in the samples.

Analyses by SEM were performed in fractured samples, on a LEICA equipment (model S440i) using a secondary electron detector (SE) and also EDS for the study of chemical elements. Analyses by X-ray diffraction (XRD) were performed on a Siemens equipment (model D5000) using the method of non-oriented mortar samples that had been previously powdered in an orbital mill.

Studies involving exudation products collected from concrete surfaces of structures (when present) were also analyzed by X-ray diffraction, as described above.

3 RESULTS AND DISCUSSIONS

Characterization of concrete core aggregates and HPP surrounding rocks

Analyses of aggregates used in the manufacture of concretes from HPPs are presented in Tables 2 and 3. ASR previous diagnoses on HPPs are also indicated. Coarse aggregates from Furnas HPPs are classified as quartzite and those from Chesf HPPs as several granitic rock types. Except for Mascarenhas HPP, the fine aggregates come just from natural sand; for the others plants, there was a

mix of natural sand and manufactured sand (from crushed rock fines). Figure 1 presents some of the main characteristics of aggregates.

According to the mineralogical analyses of the concrete aggregates, those from Chesf HPPs stand out with strained quartz and alkaline feldspar. PAII and Moxotó also indicate some feldspar portions with myrmekitic intergrowth. Quartzite from Furnas presented potentially reactive elongated quartz crystals and sutured boundaries while Mascarenhas additionally had microcrystalline quartz veins. Fine aggregate from all concretes also contain strained quartz and especially the one from Moxotó indicates microcline with graphic intergrowths of quartz. Undulatory extinction angle was just measured to indicate the potential of reactivity. According to Fournier and Bérubé [7], there are two categories of ASR depending on silica form: the first involving poorly crystalline or metastable silica minerals and the second related to quartz-bearing rocks that incorporate very fine-grained quartz or some varieties of macrogranular quartz, including deformation. RILEM AAR-1 [8] also indicates strained quartz and microcrystalline quartz as potentially reactive siliceous constituents in a rock (i.e. granite and quartzite). From the point of view of potential for ASR, all of aggregates (coarse and fine) contain reactive constituents, with some specific variations. Main Brazilian aggregates are known to be slowly reactive aggregates due to the presence of strained quartz. Some researchers also indicate this characteristic for their reactive rocks [9]. Jensen [10] gives an interesting suggestion to divide AAR classification into three subgroups: 1) very fast reactive AAR, 2) fast reactive ASR and 3) slow reactive ASR. All rocks from this paper can be included in this third subgroup. In addition, Sims et al. [11] and Jensen [10] comment it is important to use petrographic examination to identify minerals potentially susceptible to alkali release. Granitic aggregates from Chesf contain k-feldspar that can be a possible alkali contributor [10] for the ASR reactions.

It is worth noting that the aggregates from Chesf also presented, from analyses of the opaques by reflected light microscope, some sulfides species, as previously indicated in [12]. The main identified sulfide in PAII and MX is pyrrhotite, followed by pyrite, chalcopyrite, bornite and covellite. In PA IV, pyrite is the main sulfide, followed by the others. As alterations from sulfides, there are limonite, bornite, covellite and clay minerals. On the other hand, aggregates from Furnas and Mascarenhas contained only pyrite in low concentrations, with minor alterations.

As mentioned above, the rocks used as aggregates in all of the studied HPPs may be classified as slow reactive ASR after Jensen [10]. So the studies conducted with the samples collect either inside the concrete or at the sites or cores of the HPPs, showed the same mineralogy, textures and features. No significant transformation was observed. The only noticeable difference was with the sulphides of the PA II, PA IV and Mx, that has presented in the concrete cores aggregates frequent signs of transformations as corroded boards and rare oxidation to limonite.

Mechanical tests of concretes

Figures 2 and 3 presents data from compressive strength and modulus of elasticity determinations and also a correlation with the curve resulting from the equation proposed by some standards (ABNT/NBR, EC-2 and CEB-FIB), and type of aggregates available for comparison. It can be seen that most of the results for the modulus of elasticity are located below the curves, with the exception of some data from Mascarenhas and PAIV-WI. One of the main consequences of ASR deteriorations in concrete is the reduction of modulus. This behavior had also been evinced by [13] for other structures at the same Chesf HPPs and by [14] at Furnas HPP.

Chemical tests

Figure 4 shows data of pH determination on concrete samples investigated by pH Meter. The results indicate all concretes present a high level of alkalinity.

In general, average values of pH are situated in usual zone for concretes. It is known concrete represents a high alkaline environment at pH between 12.5 and 13.5. Furthermore, saturation pH of calcium hydroxide is about 12.4, according Jennifer et al. (2007). Thus, alkaline reserve of studied concretes seems to be in a good zone, as expected, in relation to the availability of calcium hydroxide. In the study, only 3 samples presented pH below 12, but above 11.5, probably due to the different locations of the drilled concretes.

Results of concrete alkalis (expressed as $\text{Na}_2\text{O}_{\text{eq}}$ - kg/m^3 of concrete) of some HPPs structures, considering contribution from all concrete constituents, are presented in Figure 5. It was intended to try to identify alkalis from all constituents of concretes, as recommended in [11,15], considering the total mass of concretes.

It is observed that the HPPs contain different levels of alkalis. PAII HPP presented the highest values of those alkalis while Mascarenhas HPP indicated the lowest one. Depending on the analysis of risk of a structure, according to ABNT NBR 15577-1 [15], there are two limits of total alkalis from concrete (considering all constituents contribution) as optional ASR mitigating measures: 3.0 kg/m³ and 2.4 kg/m³ for minimum and moderate preventive actions, respectively. If there is a need of a strong mitigating measure, alkalis cannot be used as a parameter, especially for hydroelectric structures. According to Sims et al. [11], the threshold for alkali content in concrete is 2.5 to 3.0 kg/m³ in the case of aggregates with high reactivity, following AAR 7.1 from RILEM [16]. For massive long-service structures, alkali level must be below 2.5 kg/m³. For all concrete studied, it was not used in the mix any type of pozzolan with cements as preventive measure, thus the data of alkalis (and the high levels) are consistent with the ASR identified along time in Chesf HPPs, according to Figure 5. For Furnas HPP, total alkali content is close to 2.0 kg/m³; on the other hand, the contents determined for concretes from Mascarenhas showed the lowest values among the concretes under study, and below about 1.0 kg/m³. Those data are exclusively from some drilled concretes and other values from other areas and structures can be found.

Expansion tests

The results from AMBT tests at 16 and 30 days are shown in Figure 6. Considering that aggregates from concrete cores and rocks (collected nearby the HPPs) showed the same mineralogy, textures and features, with no significant transformation, expansion results were then compared. The behaviour observed is very interesting and is repeated for all aggregates from Chesf HPPs. All potential expansions are low (< 0.06%) and remain below the threshold for considering aggregates potentially reactive (<0.19% at 30 days by Brazilian Standard NBR 15577 [15] or <0.20 % at 16 days by ASTM C-1260 [6]). In other words, the AMBT method showed **false negative results** for all aggregates considering that concretes from those Chesf power plants are affected by the AAR. Similar behavior was already observed by [13].

For aggregates from Furnas HPPs, the results were positive in indicating ASR potential for both expansions and being coherent with diagnosis done a long time ago. The average results of the tests indicate 0.47% and 0.52% expansion at 16 days in AMBT for Furnas and Mascarenhas aggregates, respectively. In both cases, the values are higher than the limits established by ASTM C-3[17], 0.20% in 16 days, or by Brazilian Standard NBR 15577/1[15], 0.19% in 30 days. It is interesting to point out expansions never stop at 16 days, indicating a slow and increasing behaviour of those aggregates up to 30 days.

Differences between expansions from core aggregates and rocks were not so expressive for the majority of the tests. Conversely, values obtained for those expansions from Moxotó appeared more distant, with almost 50% of difference at 30 days, and this behavior lasted the entire test. This behavior is compatible with the high initial expansion rate indicated by the instrumentation of the structure in this HPP and its gradual reduction observed over time.

It is clear that granitic rocks showed some limitation in the AMBT performance, even if tests last 30 days once Chesf HPPs suffer from ASR. Otherwise, quartzite rocks presented a good application of this test indicating their real potential and corroborating with concrete structures behavior and ASR diagnostic. False negative results from AMBT are well known to occur when testing granitic rocks. Several standards, including CSA and ASTM standards, suggest that the AMBT is not an appropriate test with granitic rocks; in this case the CPT could be more appropriate. Unfortunately, the program of study could not contemplate CPT at this moment; further researches must continue.

Petrographic investigations on concretes and gels

The most recurrent feature in all concrete cores investigated is the presence of voids containing material inside them, mostly whitish deposits. Sometimes the voids were only lined with those materials while others were completely filled; at times, voids appeared to have just some localized deposits. Dark stains were seen through the concrete mortars, especially at Furnas concretes. Changes in aggregates could also be seen in the signs of oxidation in Chesf concretes. Finally, rims around the aggregates were present in the majority of concretes. Except for Moxotó HPP, all the other HPP presented exudation products suggestive of gel at concrete surfaces during the field inspections. Furnas and Mascarenhas were the HPPs with the most incidences of those products. In the others, exudation products rarely appeared, and only locally.

SEM/EDS analyses generally point to some areas with normal microstructural characteristics to be found in concrete, including empty voids. In other regions, however, powdered secondary

deposits were found in addition to products of chemical alteration seen in the various crystalline sulfate phases, as well as crystalline alkali-silicate crystals and non-crystalline (amorphous) ASR gel. These products were present in various areas on the samples, whether deposited in the voids, on the cracked surfaces of the aggregates particles, on the paste-aggregate interface, or even scattered across the paste. In those voids, white material was identified through visual examination and it was always associated with the aforementioned neoformed products. Figure 7 presents some micrographs of the concretes that were investigated, showing the products detected. It is worth noting that all products shown in the figures were undergone EDS analyses. Some spectra are also presented in Figure 8.

The qualitative X-ray diffraction analyses (XRD) conducted on mortar samples from concretes showed, in majority, common phases present in the cement paste and from aggregate minerals. Calcium silicates, calcium hydroxide and calcite are present in all concretes. Monosulfate was detected in some PA IV and Moxotó concretes. Table 4 lists the main constituents identified for mortar samples Ettringite was identified in almost all concretes; gypsum was also detected, but just in the samples from the three Chesf HPPs, indicating the presence of a non-common sulfate phase.

Considering the X-ray diffraction analyses performed on samples of exudations products, their ASR origin was established by the amorphicity showed in the diffractogram obtained due to the high reflection in about 26° of 2-theta angle in all samples. In addition, there are regions indicating the presence of amorphous SiO_2 . Sometimes, associated to it is trona (T - just in PAII) - a hydrated sodium carbonate signaling excessive alkalis in the system (see Figure 5) – and traces of quartz (Q - in PAIV), calcite and feldspar (C, F - PAII), as well. Figure 9 indicates those characteristics of the exudations products studied, indicating the presence of ASR gel.

In summary, all concretes studied from some structural elements of the five HPPs contain phases resulting from chemical alterations taking place in the concretes, as shown in the SEM/EDS and XRD analysis. Concretes from Furnas and Mascarenhas presented ASR phases and HPPs from Chesf have indicated both ASR and sulfate phases.

4 CONCLUSIONS

The studies conducted and presented in this manuscript indicate a current overview of investigations carried out in some concretes of five Brazilian hydroelectric plants from Chesf and Furnas.

It is clearly noticed the negative influence of ASR on the modulus of elasticity, which reflects the deleterious chemical reactions taking place inside the concretes. For Chesf HPPs, the expansion tests (AMBT) were not able to indicate ASR potential of their concrete aggregates since they come from granitic rocks, although their mineralogical characteristics do indicate this. By contrast, quartzitic aggregates from Furnas HPPs are indicative of reactivity materials both from expansion tests and petrographic analyses. The expansions tests indicate the aggregates inside concretes can still react over time. Furthermore, expansions do not cease in the AMBT along time, indicating that aggregates are slowly reactive. The analyses from SEM and XRD conducted on concrete samples from Chesf HPPs showed the presence of phases originating both from the alkali-aggregate reaction and sulfate attack, suggesting that the negative impact on the modulus may not originate exclusively from the ASR. The presence of gypsum suggests an internal sulfate attack. On the other hand, it was verified a minor incidence of just ettringite at Furnas HPPs, and punctually, indicating those concretes suffer only by ASR. Chemical analyses performed indicated total alkalis content vary along the structures/HPP. Concrete from PAII presented the major alkalis content, exceeding 4 kg/m^3 of $\text{Na}_2\text{O}_{\text{eq}}$; on the other hand Mascarenhas showed the lowest one. In general, pH is situated in usual zone for all concretes.

Finally, the studies undergone at Chesf HPPs as reported in this manuscript indicated that a new attack front may exist from sulfides besides ASR. At Furnas HPPs, the attack seems to be solely by ASR acting up nowadays, with less important consequences. Field investigations will continue over time with complementary studies to enable monitoring performance of concretes and its durability and, eventually, some interventions.

5 REFERENCES

- [1] ABNT NBR 15577-3 (2008): Agregados - Reatividade Álcali-Agregado - Parte 3: Análise Petrográfica para Verificação a Potencialidade Reativa de Agregados em Presença de Álcalis do Concreto. Associação Brasileira de Normas Técnicas, São Paulo.
- [2] ASTM C 39 (2012): Standard test method for compressive strength of cylindrical concrete specimens. American Society for Testing and Materials, West Conshohocken.
- [3] ASTM C 469 (2010): Standard test method for static modulus of elasticity and Poisson's ratio of concrete in compression. American Society for Testing and Materials, West Conshohocken.

- [4] Jennifer, AG, Hemants, SL and Ashok, MK (2007): Testing pH of Concrete - Need for a standard procedure. *Concrete International*, 6p.
- [5] ABNT NBR 15577-4 (2009): Agregados - Reatividade Álcali-Agregado - Parte 4: Determinação da Expansão em Barras de Argamassa pelo Método Acelerado. Associação Brasileira de Normas Técnicas, São Paulo.
- [6] ASTM C 1260 (2014): Standard Test Method for Potential Alkali Reactivity of Aggregates (Mortar-Bar Method), West Conshohocken.
- [7] Fournier, B and Bérubé, MA (2000): Alkali-aggregate reaction in concrete: a review of basic concepts and engineering implications. *Can. J. Civ. Eng.* 27: 167-191.
- [8] RILEM AAR-1 (2003): Rilem Recommended test method AAR-1: Detection of potential alkali-reactivity of aggregates – Petrographic method. By I. Sims and P. Nixon. *Materials and Structures*. 36: 480-496.
- [9] Shayan, A, Xu, A and Morris, H (2008): Comparative study of the concrete prism test (CPT 60°C, 100% RH) and other accelerated tests. In: Broekmans, MATM and Wigum, BJ (editors): *Proceedings of 13th ICAAR - International conference of alkali-aggregate reaction in concrete*, June 16–20, 2008, Trondheim, Norway: 412-421.
- [10] Jensen, V (2012): Reclassification of alkali aggregate reaction. In: *Proceedings of 14th ICAAR - International conference of alkali-aggregate reaction in concrete*, May 20–25, 2012, Austin, Texas: 1-10.
- [11] Sims, I, Nixon, P and Godart, B (2012): Eliminating alkali-aggregate reaction from long-service structures. In: *Proceedings of 14th ICAAR - International conference of alkali-aggregate reaction in concrete*, May 20–25, 2012, Austin, Texas: 1-12.
- [12] Hasparyk, NP, Silva, PN, Batista, DG, Silva, HH, Cavalcanti, AJ and Carasek, H and Andrade, M. (2008): Current studies on HPPs from the Paulo Afonso Hydroelectric Complex in relation to the quality and durability of concretes. In: *Dam World Conference. Proceedings of 54th Congresso Brasileiro do Concreto*, 2012, Macció, Brazil: 1-17.
- [13] SILVA, PN (2007): Alkali-aggregate reaction at the Paulo Afonso Hydroelectric Complex - CHESF. Influence of the reaction in the properties of the concrete. MSc. Dissertation (in portuguese), Universidade Federal de São Paulo – USP, São Paulo/SP, 220p.
- [14] Hasparyk, NP (2005): Investigation of concretes affected by alkali-aggregate reaction and advanced characterization of exuded gel. PhD Thesis (in portuguese), Universidade Federal do Rio Grande do Sul - UFRGS, Porto Alegre/RS, 326p.
- [15] ABNT NBR 15577-1 (2008): Agregados - Reatividade Álcali-Agregado - Parte 1: Guia para Avaliação da Reatividade Potencial e Medidas Preventivas para uso de Agregados em Concreto. Associação Brasileira de Normas Técnicas, São Paulo.
- [16] RILEM Recommended Specification (2016): AAR-7.1 – International specification to minimize damage from alkali reactions in concrete – Part 1: Alkali-silica reaction.
- [17] ASTM C 33 (2013): Standard specification for concrete aggregates. American Society for Testing and Materials, West Conshohocken.
- [18] ABNT NBR 6118:2014 (2014): Projeto de estruturas de concreto — Procedimento, São Paulo.
- [19] CEB-FIP Model Code 2010 (2012): Bulletin n.65, Switzerland.
- [20] EN 1992-1-1, Eurocode 2 (2004): Design of concrete structures.

TABLE 1: Concrete cores drilled from HPPs and abbreviations.

HPP	N. of cores	Drilling site
Furnas (F)	3	Spillway (S)
Marechal Mascarenhas de Moraes (M)	10	Water intake (WI)
Paulo Afonso II (PAII)	6	Water intake (WI)
Paulo Afonso IV (PAIV)	5	Water intake (WI)
	5	Spillway (S)
Moxotó (Mx)	8	Downstream Powerhouse

TABLE 2: Concrete aggregates from Furnas and main petrographic/mineralogical characteristics.

HPP	Type	Classification	Mineralogical Characteristics	Potential Features	HPP ASR Diagnosis
F	Coarse	Quartzite	Major constituents: quartz. Accessories: sericite and opaque.	Elongated quartz crystals, quartz with irregular (sutured) boundaries and frequent strained quartz with UE of 20-30°.	Yes
	Fine	Natural and manufactured sands from quartzite	Major constituents: quartz and quartzite fragments. Accessories: opaque, feldspar, mica, sillimanite, tourmaline.	>50% of strained quartz with UE of 20-30°.	
M	Coarse	Quartzite	Major constituents: quartz. Accessories: sericite, opaque and titanite.	Mortar texture with up to 90% of strained quartz with UE of 30°. Microcrystalline quartz veins (5-15%).	Yes
	Fine	Natural sand	Major constituents: quartz. Accessories: opaque, feldspar, tourmaline, titanite, zircon.	5% of quartz with UE of 15-30°.	

Note: UE: undulatory extinction angle in the quartz grains.

TABLE 3: Concrete aggregates from Chesf and main petrographic/mineralogical characteristics.

HPP	Type	Classification	Mineralogical Characteristics	Potential Features	HPP ASR Diagnosis
PAII	Coarse	Granitic rocks (Biotite granite, diorite and granodiorite)	Major constituents: plagioclase, quartz, microcline. Accessories: biotite, opaque, epidote, titanite, muscovite, carbonate, chlorite, zircon, apatite.	15 to 30% of strained quartz with UE from 10 to 30°. Some myrmekite: intergrowth by quartz in plagioclase.	Yes
	Fine	Natural quartz sand and manufactured sand from granitic rocks	The same above and also rounded quartz grains from natural sand.		
PAIV	Coarse	Granitic rocks (Biotite granite, leucogranite and hornblende granite)	Major constituents: plagioclase, microcline, quartz, biotite. Accessories: apatite, zircon, opaque, titanite, carbonate.	80 to 90% of strained quartz with UE of 20 to 30°.	Yes
	Fine	Natural quartz sand and manufactured sand from granitic rocks	Major constituents: quartz and feldspars with opaque and biotite as accessories.	60 to 80% of strained quartz with UE from 20 to 30°.	
Mx	Coarse	Granitic rocks (Biotite granite and granodiorite)	Major constituents: plagioclase, quartz, microcline, biotite. Accessories: amphibole, opaque, epidote, titanite, chlorite, carbonate, zircon, apatite.	15 to 40% of strained quartz with UE from 20 to 30°. Fine-grained interstitial aggregates of quartz, feldspars and biotite with some polygonal grains forming triple junctions and, indicating recrystallization. Little myrmekitic intergrowth.	Yes
	Fine	Natural quartz sand and manufactured sand from granitic rocks	The same above and also rounded quartz grains from natural sand.	The same deformation above. It was also observed a graphic intergrowth of quartz in microcline at a pegmatite fragment.	

Note: UE: undulatory extinction angle in the quartz grains.

TABLE 4: Summary of the main phases identified by XRD in the concrete pastes.

Phase / HPP	F	M	PA II	PA IV	Mx
C-S-H	x	x	x	x	x
CH	x	x	x	x	x
Calcite	x	x	x	x	x
Ettringite	x	x	x	x	x
Monosulfate				x	x
Gypsum			x	x	x

Legend: CH: Portlandite; C-S-H: Hydrated calcium silicate.

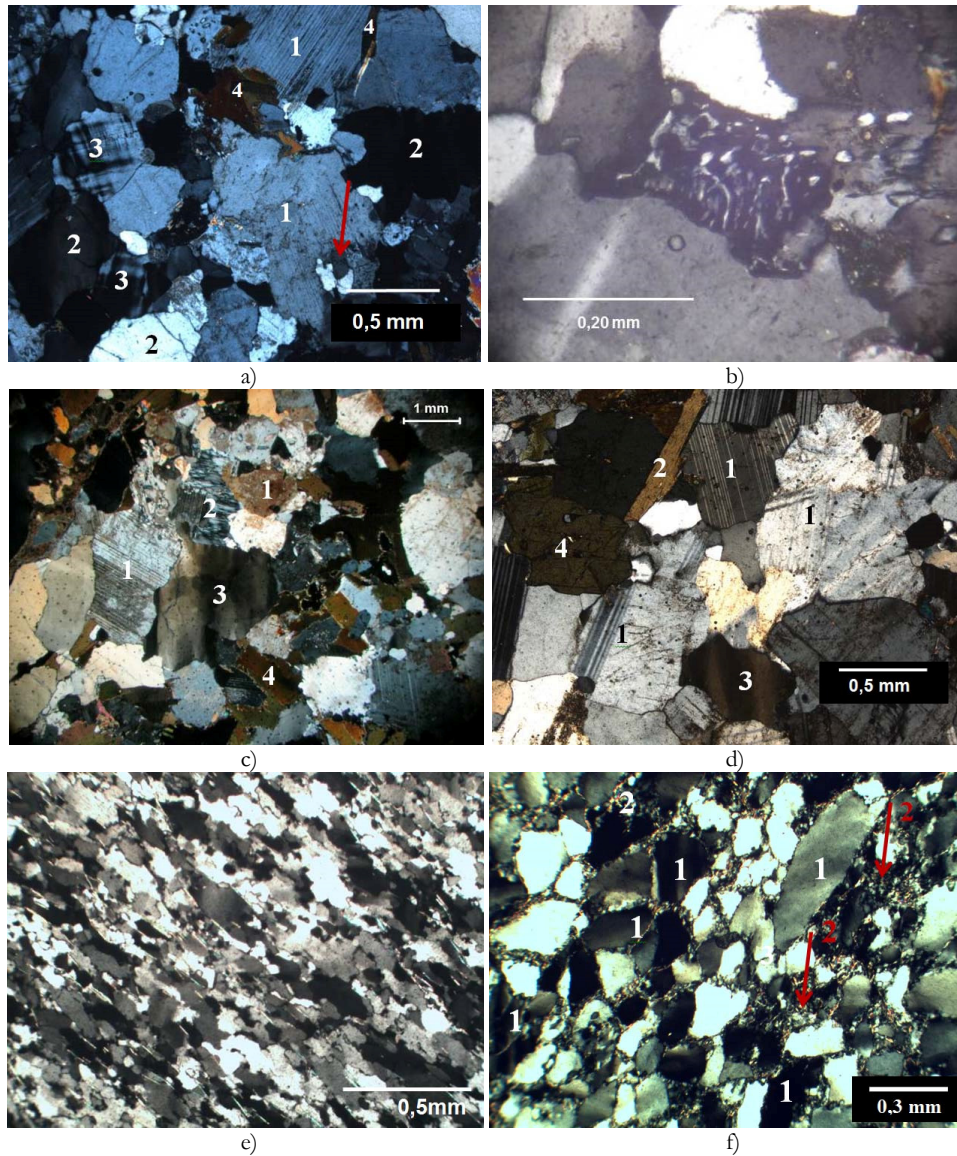


FIGURE 1: Optical micrographs, XPL-cross polarized light (polarized light microscope) of coarse aggregates from HPPs: a) PAII - Biotite granite: plagioclase (1), quartz (2), microcline (3), biotite (4) and fine-grained quartz inclusions in plagioclase (arrow). b) PAII - Biotite granite: myrmekite at the center. c) PAIV- Biotite granite: plagioclase (1), microcline (2), strained quartz (3), with restricted biotite (4). d) Moxotó - Granodiorite: plagioclase (1) with biotite (2) and strained quartz (3); amphibole (4) is rare. e) Furnas - Quartzite: frequent elongated and strained quartz crystals with irregular (sutured) boundaries and very fine oriented lamellae of sericite with preferential orientation. f) Mascarenhas - Quartzite: mortar texture with high undulatory extinction in quartz grains cemented by microcrystalline quartz (arrows) and association to small-sized sericite lamellae (colored particles).

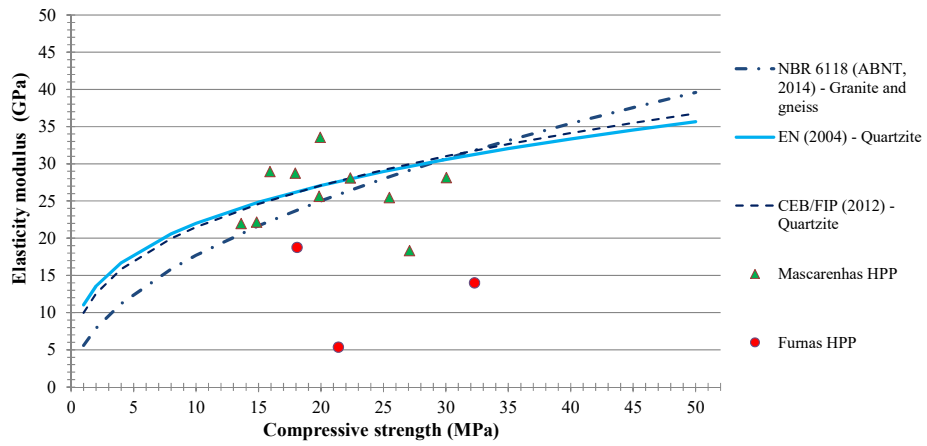


FIGURE 2: Correlation between compressive strength and modulus of elasticity of the concrete cores from Furnas HPPs.

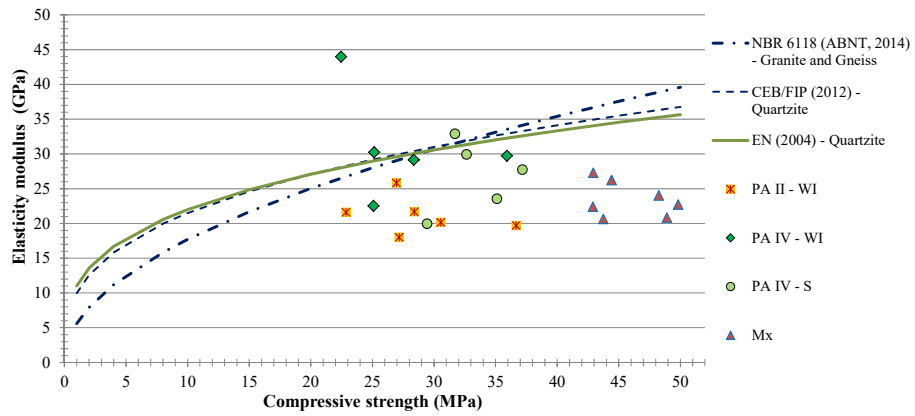


FIGURE 3: Correlation between compressive strength and modulus of elasticity of the concrete cores from Chesf HPPs.

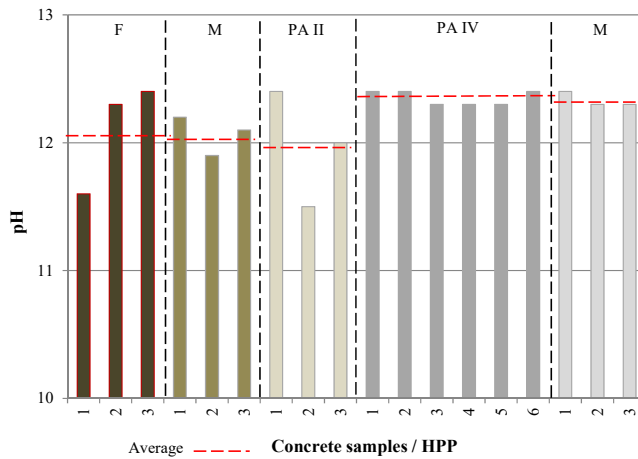


FIGURE 4: pH of concretes.

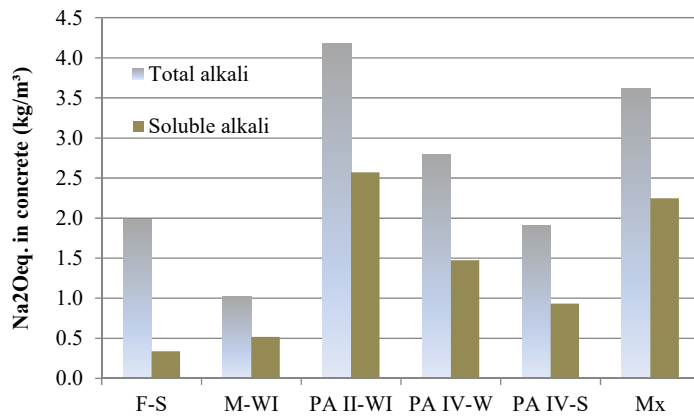


FIGURE 5: Level of alkalis (in kg/m³) in the concretes.

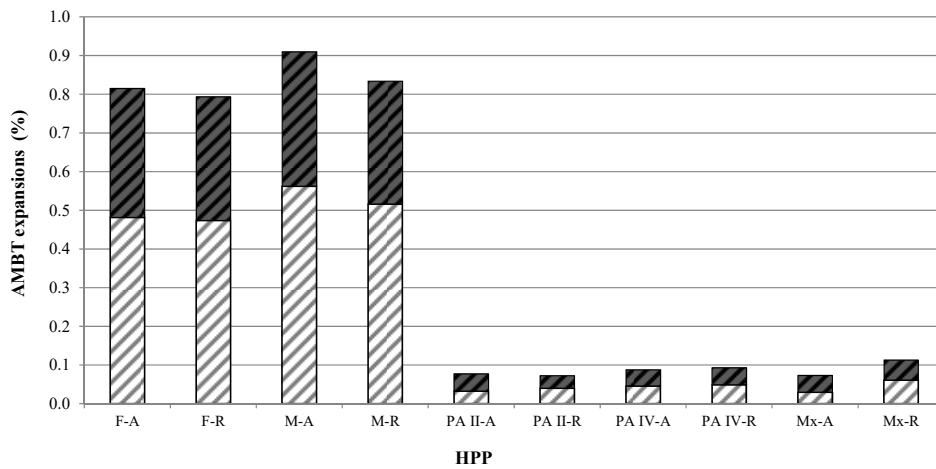
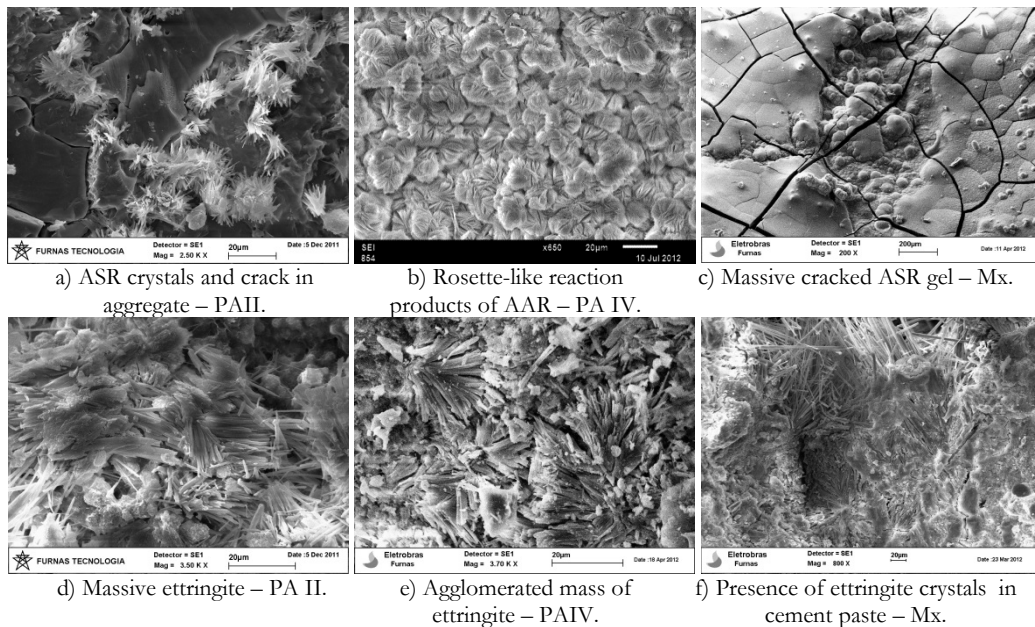
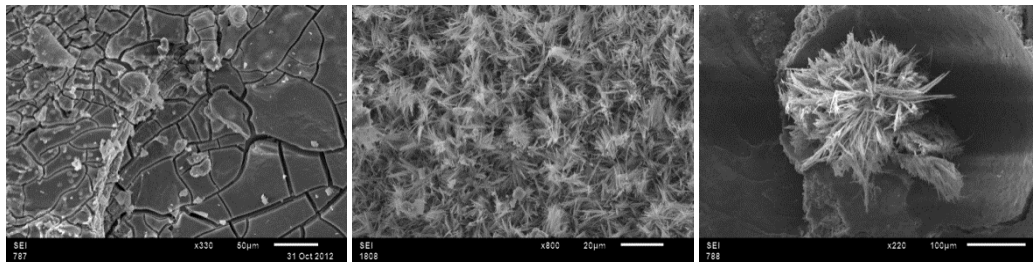


FIGURE 6: Expansive behavior of the HPPs' aggregates (A) from concrete cores and rocks (R) by AMBT.

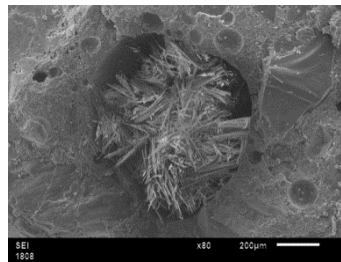




g) Massive and cracked ASR gel - F.

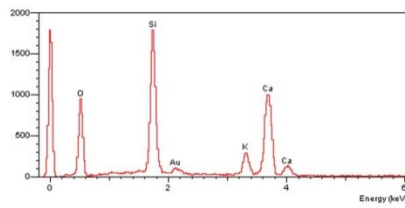
h) Crystals from ASR - M.

i) Ettringite in the pore - F.

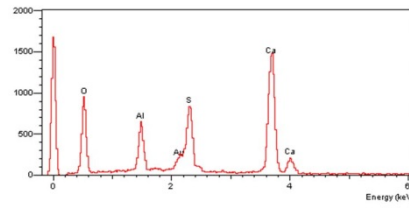


j) Pore filled with ettringite - M.

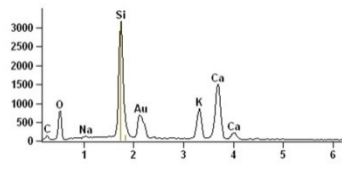
FIGURE 7: SEM images and EDS spectrum.



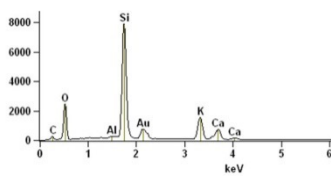
Spectrum from Figure 7c



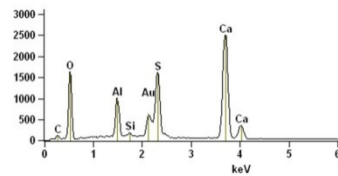
Spectrum from Figure 7d



Spectrum from Figure 7g



Spectrum from Figure 7h



Spectrum from Figure 7j

FIGURE 8: EDS spectra.

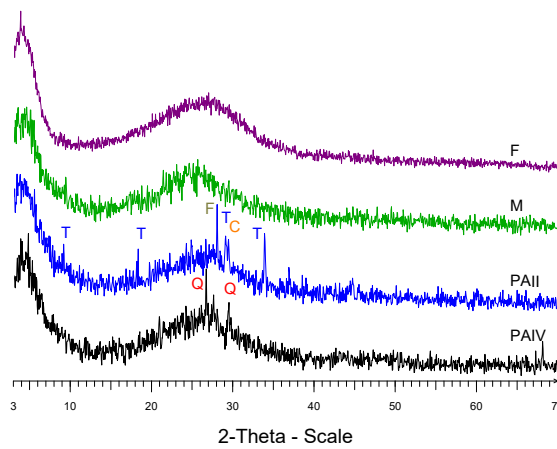


FIGURE 9: X-ray diffractograms of ASR Gels.